doi:10.26443/seismica.v5i2.2182

SEISMICA

Shallow subsurface imaging from footsteps recorded by DAS

T. W. Luckie [*] [1], **R. W. Porritt** [1], **A. C. Stanciu** [1]

[1]Sandia National Laboratories, Albuquerque, New Mexico, USA

Author contributions: *Conceptualization*: TWL, RWP, ACS. *Data Curation*: TWL, RWP. *Formal Analysis*: TWL. *Funding Acquisition*: RWP, ACS. *Investigation*: TWL. *Methodology*: TWL. *Project Administration*: RWP, ACS. *Resources*: RWP, ACS. *Software*: TWL. *Supervision*: RWP, ACS. *Validation*: TWL. *Visualization*: TWL. *Writing – original draft*: TWL. *Writing – review & editing*: TWL, RWP, ACS.

Abstract Characterizing the shallow subsurface seismic structure is essential for a broad spectrum of geophysical analyses, including seismic event detection, ground motion monitoring, and the assessment of anthropogenic activities. However, data collection in urban areas is often constrained by practical or logistical challenges associated with the deployment of sources and receivers, particularly in scenarios requiring dense seismic data acquisition. This study seeks to address the practical limitations of traditional seismic sources in urban areas by utilizing footsteps as a novel data source recorded by distributed acoustic sensing (DAS). We show that footstep-generated seismic waves can be effectively used to calculate shear wave velocities and perform reflection imaging of the shallow subsurface. By inverting dispersion curves from footstep data, we generated a 2-D shear wave velocity profile, which was compared to an existing 3-D model obtained from conventional active sources. Our results indicate that footstep sources can provide high-resolution subsurface imaging to depths of ~25 m, enhancing seismic models in urban environments where traditional methods may be less practical. This innovative approach offers a potential solution for improving our understanding of subsurface structures in earthquake-prone regions.

Non-technical summary Understanding the structure of the Earth beneath urban areas is crucial for assessing earthquake risks. Traditional methods of collecting seismic data often face challenges in densely populated settings. In this study, we explored a new approach by using footsteps as a source of seismic waves, recorded through distributed acoustic sensing (DAS). We found that these footsteps can help us create detailed calculations of the structure and properties of the shallow subsurface. Our findings suggest that using footsteps can provide valuable information about underground structures, which is essential for improving safety measures in cities at risk of earthquakes. This method is not only innovative but also offers a more accessible way to gather seismic data in urban environments.

Production Editor:
Andrea Llenos
Handling Editor:
Wenbo Wu
Copy & Layout Editor:
Kirsty Bayliss

Signed reviewer(s):
Haipeng Li

Received:
December 8, 2025
Accepted:
June 12, 2026
Published:
July 23, 2026

1 Introduction

Characterizing shallow wave speeds in the upper 30 m of the Earth (i.e., Vs30 calculations; McPhillips et al., 2020) provides valuable data for various applications, such as seismic monitoring, modeling very-near source wave propagation, or seismic hazard analysis, among others. Vs30 is necessary for understanding ground motions from waves generated by seismic sources, but it can also improve hyper-local seismic wave propagation models. Models of very shallow seismic structure can also complement larger Earth models, benefitting analyses like source detection, discrimination, and location. Efforts to collect data in urban areas for such models can encounter practical or logistical limitations in source and/or receiver placement. Distributed acoustic sensing (DAS), which utilizes fiber-optic cables as a series of vibrational sensors, can collect seismic data at high spatiotemporal resolutions (Lindsey and Martin, 2021). Fiber-optic cables are ubiquitous in urban settings where researchers may have limited access to install sensors in urban environments. Thus, DAS provides a unique opportunity for in situ means of collecting data. DAS has been used to characterize the shallow subsurface, demonstrating its potential for calculating subsurface wave speeds (Fukushima et al., 2022; Liu et al., 2022; Zhou et al., 2022; Hong et al., 2024; Li et al., 2025) and imaging reflectivity (Wu et al., 2017).

While dense instrumentation in urban areas can be achieved using DAS, sources may be limited. Passive sources (e.g., ambient noise or teleseisms) may not have the correct frequency content to resolve the upper 30 m of the subsurface. Active sources (e.g., weight drops or vibroseis) in urban environments may be difficult or impossible to execute due to practical or logistical barriers. Thus, to fully leverage urban DAS to create high resolution images of the shallow subsurface, an alternative and widely available opportunistic source is needed. Footsteps are a suitable candidate source that can be recorded by DAS (e.g., Kang et al., 2025; Yuan et al., 2025; Zhou et al., 2024; Jakkampudi et al., 2020) in urban settings. They can be located using back-projection with similar accuracies to GPS when occurring within ~24 m

*Corresponding author: twlucki@sandia.gov

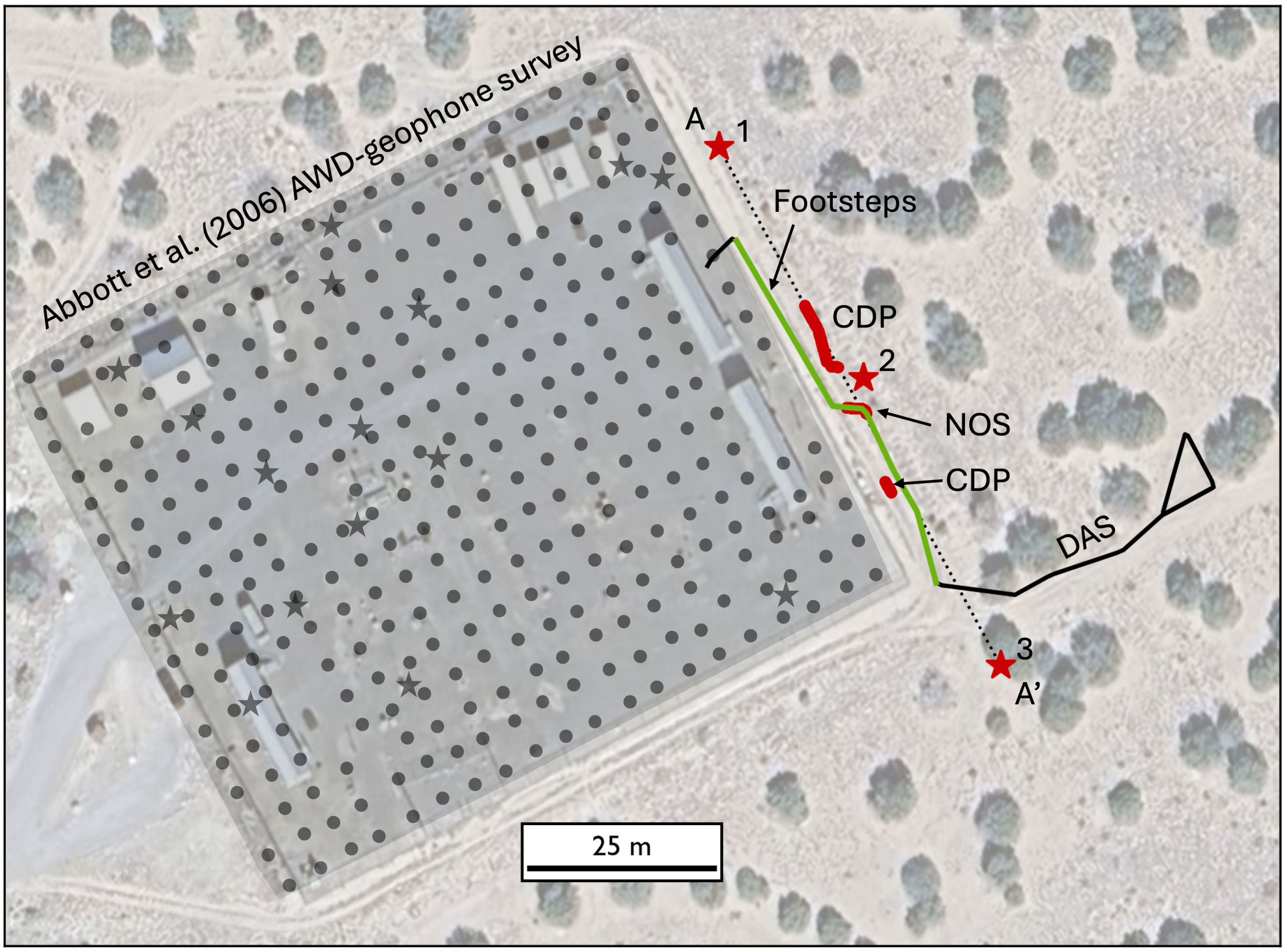

Figure 1 Basemap satellite image of the Facility for Acceptance, Calibration, and Testing (FACT) site showing DAS fiber (black line), footstep path (green line), AWD locations recorded by DAS (numbered stars), and reflection locations (red lines). The footprint of the 3-D survey by Abbott et al. (2006) is shaded in gray with their geophones (circles) and AWD sources (stars) marked. The A-A' profile used in this study is shown as a dotted line. CDP – common depth point; NOS – near offset.

of a fiber (Luckie et al., 2025), allowing their use as a hybrid passive-active source in seismic analysis.

Here, we demonstrate the use of footstep sources to perform shallow shear wave speed (Vs) calculations by inverting dispersion curves. We also use the energy generated by footsteps to perform reflection imaging of the shallow subsurface. For ground-truth, we compare our results to an existing 3-D Vs model, assembled using accelerated weight drop (AWD) sources recorded by a 2-D array of geophones (Abbott et al., 2006). We compare a reflection profile calculated using footstep arrivals to a synthetic reflection profile calculated from our Vs model. Our results show that we can generate high-resolution wave speed models of the subsurface in urban environments using footsteps recorded by DAS, providing a means to improve seismic wave speed models in areas difficult to instrument.

2 Data collection

DAS data were collected at Sandia National Laboratories' (SNL) Facility for Acceptance, Calibration, and Testing (FACT) site (Figure 1). The DAS interrogator was a Silixa iDAS-MG collecting data along a 142 m long single-mode armored cable. The sampling frequency was 1000 Hz with a gauge length of 3 m and virtual channel spacing of 0.25 m. The fiber installation was, in order from the interrogator unit: 10 m on the surface, 10 m buried in concrete, 10 m buried in grout, and 10 m inside a buried rain gutter. The remaining fiber length was directly buried ~0.25 m below ground surface. Previous studies using this data did not see an appreciable effect of coupling or burial type on the recorded footstep arrival amplitudes (e.g., Luckie et al., 2025).

A ~50 m path of footsteps running parallel to the fiber were used as sources for this analysis (Figure 1). Footsteps followed a normal walking gait and pace (Luckie et al., 2025). The walking path and DAS fiber run parallel to the northeast edge of the FACT site. The path followed an unpaved, graded road. A total of 53 footsteps were recorded along this segment (Figure 2). Individual footstep data gathers containing 40 channels were manually cut from the DAS recordings and high-pass filtered above 1 Hz for downstream processing. The spacing of these footsteps permit reflection imaging of a common depth point (CDP) profile. For additional ground truth of our results, three AWD shots were recorded by DAS (Figures 1,3). Note that these AWD sources are different from the AWD-geophone survey of Abbott et al. (2006). These AWD-DAS data permitted two sections of CDP and one section of near-offset (NOS) imaging (Figure 1). Because of the sparse spacing of these AWD sources, only a coarse CDP was possible for this source-receiver geometry.

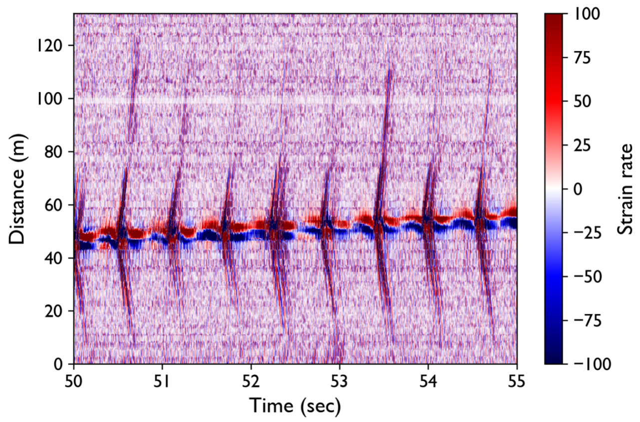

Figure 2 Five-second window of DAS data showing a series of footprint arrivals (amplitude is nano strain rate).

The power spectral densities of the AWD and footstep sources as recorded by DAS show patterns which can influence subsequent wave speed calculations. In particular, the AWD spectrum shows higher power for frequencies <10 Hz compared to the footstep spectrum (Figure 4). These lower frequencies contain more low phase velocity information (Park et al., 1998), potentially depressing any resulting shear wave speeds calculated using footstep sources compared to AWD sources. This difference in source frequency content will carry over from DAS (i.e., this study) to geophone (i.e., Abbott et al., 2006) data.

3 Wave speed calculation

We inverted individual 1-D Vs functions from dispersions curves of each footstep, which were then stitched together to create a 2-D Vs profile. The multi-channel analysis of surface waves (MASW) method of Park et al. (1999) was used to calculate frequency-velocity spectra of footstep data gathers (Figure 5A). For each frequency bin in the MASW calculation, the peak amplitude was automatically picked to find the dispersion curve for that footstep source. Individual spectra and dispersion curves were manually inspected for quality control. A total of 10 incoherent spectra or unsuitable dispersion curves were removed from further analysis, after which 43 footstep dispersion curves remained.

Dispersion curves were inverted for a 1-D isotropic layered velocity function using the evolutionary algorithm of Luu (2023). This method functions similar to a Monte-Carlo based method in that it is stochastic in nature and is an iterative process. However, evolutionary algorithms mutate the candidate solutions between iterations to arrive at the best fitting solution in the solution space (Luu, 2023). Evolutionary algorithms are thus better optimized than Monte-Carlo methods to search for solutions, can explore more solutions to avoid local optima, and are generally more robust to noise in the evaluation of solutions (Bäck and Schwefel, 1993).

We used a maximum of 1000 iterations, with each iteration evaluating 10 possible solutions, for a total of 10,000 models evaluated. These values were chosen for convenience and computational efficiency of the evolutionary algorithm. The model search boundaries allowed for 10 layers with a variable thickness between 1-25 m and variable velocities between 50-800 m/s, with the deepest layer as a half-space. Layer thickness and velocities were adjusted in each iteration to fit the data. The result with the lowest RMS was chosen as the best fit model. An example of an inverted 1-D Vs function is shown in Figure 5B. The resulting series of 1-D Vs functions were concatenated and interpolated to form a 2-D Vs profile (Figure 6A). This profile was interpolated using a Gaussian window to smooth between 1-D functions and fill-in gaps in footstep coverage due to poor dispersion curve quality.

For ground truth, we compare our model with the 3-D Vs model of Abbott et al. (2006). This experiment used a series of AWD sources recorded by a 2-D array of 4.5 Hz vertical component geophones sampling at 1000 Hz covering the FACT site (Figure 1). Like our analysis, Abbott et al. (2006) inverted dispersion curves for shear-wave velocities using a stochastic, iterative process. Their method refines a starting model through random perturbations and inversion, aiming to minimize RMS error and escape local minima, with the process flagged as incomplete if the global error limit is not achieved after 60 iterations. While similar to evolutionary algorithms, their method is slightly different in the way it explores the solution space for the best fitting model. In both cases, however, a range of possible solutions are evaluated with the best fitting model chosen for that particular dispersion curve. We extracted the nearest portion of their 3-D model which matched the distribution of our 2-D profile for direct comparison between Vs calculations (Figure 6B).

4 Reflection calculation

In typical applications, CDP involves evenly spaced sensors recording evenly spaced sources in a linear geometry to calculate a reflection profile. We use DAS channels and footsteps to replicate this regular geometry. Data are organized by traces with the same midpoint rather than by receiver or source number to create CDP gathers. Relative geometries of a CDP reflection profile can be organized into stacking charts which represent source locations relative to receiver locations in surface stacking charts (Figure 7A) and source locations to midpoint locations in subsurface stacking charts (Figure 7B). The number of traces (n) sampling a specific CDP represents the n-fold multiplicity of the gather. The fold naturally falls off near the edges of the profile. In the case of the footstep-DAS data, the profile has a maximum 42-fold stack (Figure 7D). Normal moveout (NMO) corrections were applied to the CDP gathers using the velocity profile calculated from dispersion curves. The

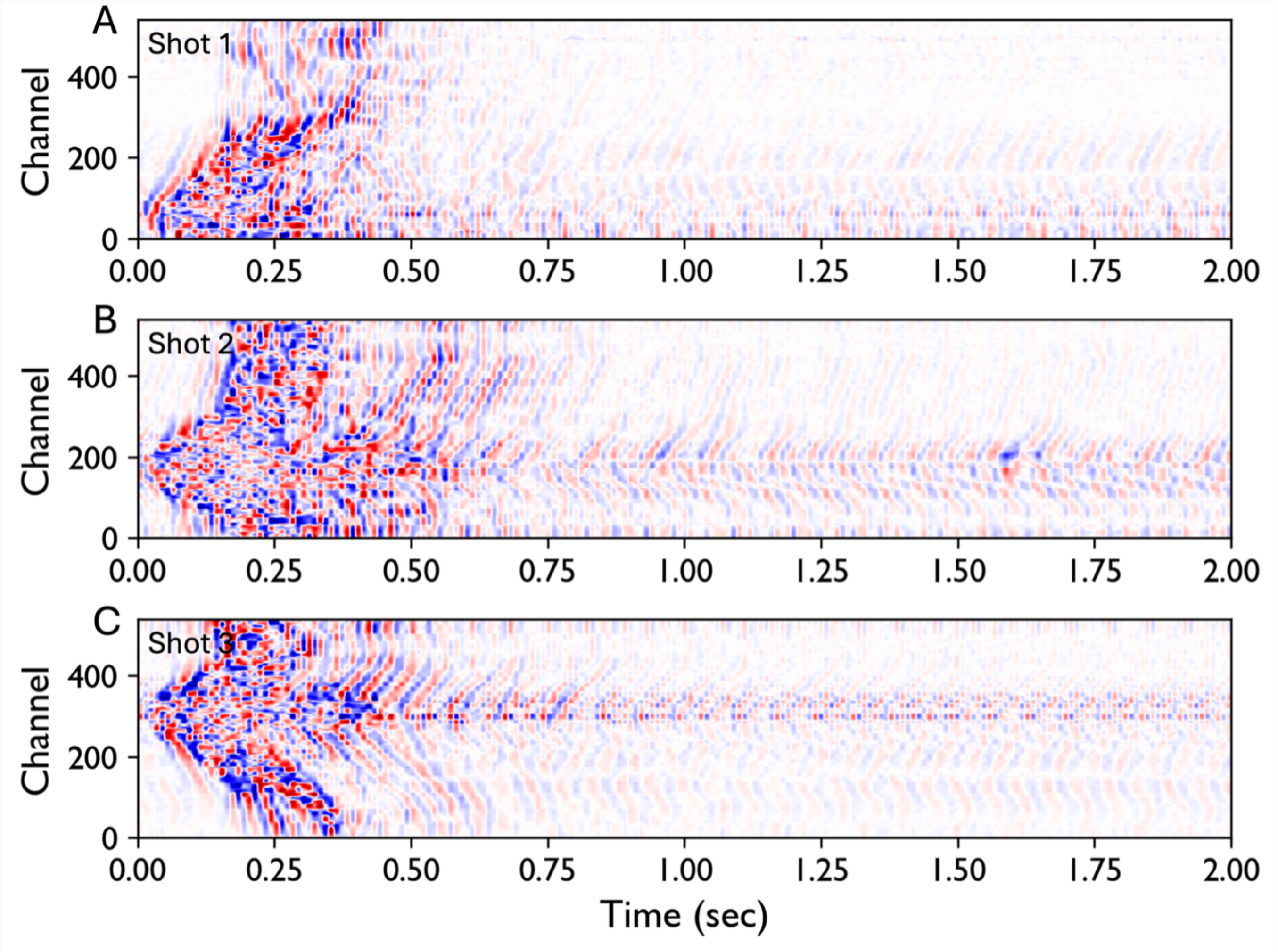

Figure 3 Data gathers of AWD shots 1 (A), 2 (B), and 3 (C). Locations are shown in Figure 1.

aligned CDP gathers were then stacked to form a trace for that CDP location. These traces were then assembled to create a reflection profile (Figure 8).

As an alternative approach, we also performed reflection imaging using the AWD-DAS data (Figures 1, 3). The sparse sources recorded by a dense array act as an analog to performing an active source survey in an area with limited accessibility. The AWD-DAS geometry yields two short segments of two-fold CDPs (~10 m and ~4 m long) and one segment of NOS (~4 m long) with significant gaps between each segment. The coverage of the AWD-DAS reflection is demonstrably worse than the footstep-DAS coverage with only a two-fold CDP possible. Despite the less-continuous nature of the AWD-DAS profile due to sparse source spacing, the AWD data does propagate deeper with higher amplitudes than the footstep-DAS data, illuminating brighter reflectors at deeper depths (Figure 8A).

Finally, to check for consistency between results, we calculated a synthetic reflection profile from the footstep 2-D Vs profile (Figure 8C). We used a 2-D finite difference forward modelling method to solve the acoustic wave equation. To artificially generate reflections from the smooth 2-D profile, a 25% velocity reduction was applied to isocontours at 100 m/s increments. A first-derivative Gaussian source with a center frequency of 100 Hz was placed at each grid node at the surface of the model. Synthetic receivers were also placed at each surface grid node. To suppress artificial multiples in the synthetic data, the model was expanded 200 m laterally and in depth. A 10-node wide absorbing boundary condition was applied to the left, right, and bottom to suppress model-edge reflections. The synthetic data was bandpass filtered from 5 to 100 Hz. The bandpass filter cutoffs and source center frequency were chosen to match the observed frequency content of the footstep reflection profile (Figure 8B). While DAS has a known azimuthal sensitivity observed in seismic arrivals (Lindsey and Martin, 2021), we do not observe such patterns in our footstep arrival amplitudes (Figure 2). This is consistent with other near-field impacts recorded by DAS (e.g., Kang et al., 2025). Thus, we do not apply azimuthal-based amplitude scaling to our synthetic calculations.

5 Results

The 2-D Vs calculation (Figure 6A) shows a generally smooth gradient with depth. Wave speeds vary from ~300 m/s near the surface to ~400-450 m/s at depth, with wave speeds resolved down to ~25 m depth. Below ~20 m depth and between ~20-45 m profile distance is

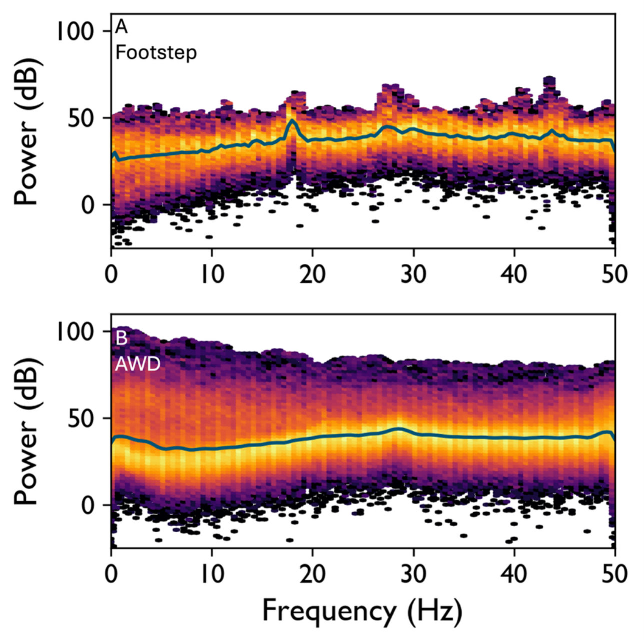

Figure 4 Comparison of power spectral densities (PSD) for footstep (A) and AWD (B) sources. Background shows the density of PSDs with the mean PSD plotted as a continuous blue line.

a region of >400 m/s wave speeds. Such a region is also seen in the AWD-geophone result of Abbott et al. (2006) at similar depths and dimensions (Figure 6B). However, the wave speeds in the Abbott et al. (2006) calculation are ~25 m/s greater than our footstep-DAS result. In general, wave speeds in Abbott et al. (2006) AWD-geophone Vs model are higher than that seen in our footstep-DAS Vs model across all depths. These velocity discrepancies are possibly due to differing sources used in each analysis or changes in shallow subsurface properties between studies.

Reflections from the footstep-DAS data reveal a set of strong, flat, and semi-continuous reflectors at ~0.1 sec two-way travel time (TWTT) (Figure 8B). Below ~0.2 sec, reflections become weak. Compared to the AWD-DAS reflection profile (Figure 8A), the footstep-DAS reflection profile provides an interpretable and coherent image of subsurface structure. While the AWD-DAS reflection energy shows ~2x stronger reflections below ~0.15 sec, the discontinuous nature of the CDP and NOS profiles, combined with very low-folds, makes this profile difficult to confidently interpret.

6 Discussion

Weak energy below ~0.2 s suggests footstep energy cannot fully propagate beyond the very near surface (i.e., ~25 m; Figures 6A, 8B). This is corroborated by the synthetic reflection profile (Figure 8C), where a strong reflector is observed at ~0.1 sec, with weak and multiple reflectors present below ~0.2 sec. Compared to the deeper propagating AWD energy (Figure 8A), this highlights that reflection profiles calculated from footstep energy are likely limited to the very near-surface. Thus, to establish validity of our results, we first compare our wave speed calculations to results from Abbott et al. (2006). After this, we interpret our results and provide a discussion of the relevance of our method in resolving the near surface seismic structure.

6.1 Comparison to previous calculations

While the Abbott et al. (2006) AWD-geophone wave speeds are generally ~25 m/s faster than our footstep-DAS Vs model, the ratio between the calculations revealed heterogeneities between results (Figure 9A). The ratio between footstep-DAS Vs to AWD-geophone Vs generally fell between 0.90 and 0.95, except for two regions >1.0 near the margins of the high Vs feature below ~20 m depth. In general, the <1.0 Vs ratios may be a result of different frequency content of the two source types (Figure 4). The >1.0 ratios suggest that our calculation is over estimating Vs compared to the Abbott et al. (2006) model in these regions. Our model's depth limit is ~5 m shallower than Abbott et al. (2006), meaning that we may be underestimating the top of this high Vs feature. The mismatch in velocities may also be due to differences in how velocities were inverted from dispersion curves. Abbott et al. (2006) fit velocities with constant layer thicknesses of 2 m, which were then smoothed using the nearest-neighbor algorithm when stitched together into a 2-D profile (Figure 6B). Using constant layer thicknesses versus variable layer thicknesses will result in slightly different velocity results. However, it may be that the differences in velocities are also due to very shallow property changes during the ~20 years between our study and Abbott et al. (2006).

When considering the RMS misfit of our Vs calculation, however, the regions of ratios >1.0 fall within low (<0.25 m/s) estimated errors (Figure 9B). Without corresponding error estimates from Abbott et al. (2006) it is difficult to fully reconcile these discrepancies. It is possible that the resolution near the edge of the Abbott et al. (2006) model, where the profile from Figure 6B is taken, could be relatively lower than the center of their model. It is also possible that the different source-receiver configurations resulted in differing frequency content (e.g., Figure 4), influencing resolved wave speeds with depth for the ratio <1.0 regions. In either case, the differences between profile wave speeds are small, mostly <~30 m/s, with footstep-DAS RMS errors mostly <~40 m/s. Furthermore, both profiles show the same general patterns, suggesting that our calculation is congruent with the Abbott et al. (2006) model.

6.2 Interpretation of subsurface structure

With the presence of a high wave speed feature in our results and Abbott et al. (2006), the question remains of what is generating this structure. Using the 400 m/s isocontour as a reference, the top of the structure would fall between 15-20 m depth (Figure 6). Migrating the reflection profiles from TWTT to depth places the bright reflector at a depth of ~18 m (Figure 8). These depths are deeper than a previously estimated boundary at 2-12 m at the FACT site (Luckie et al., 2025) but shallower than the estimated depth to bedrock at ~40 m (Abbott et al., 2006). Footstep energy propagating 40 m to bedrock

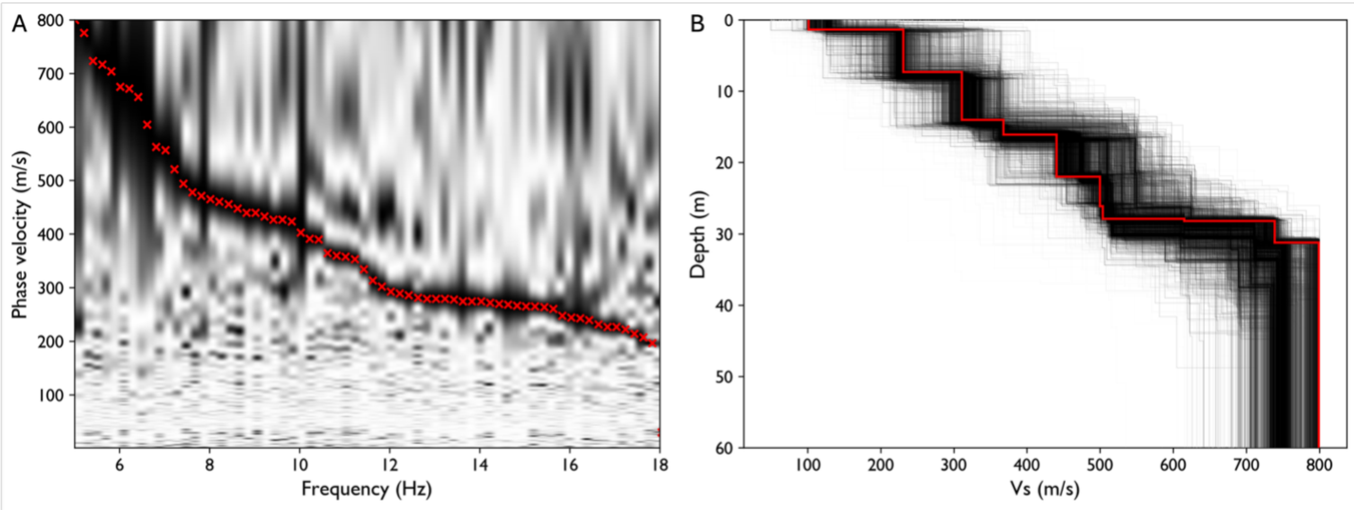

Figure 5 Graphical example of wave speed inversion. First, a sample frequency-velocity spectrum from MASW for a footstep source is calculated (A). The dispersion curve is taken as the maximum amplitude at each frequency bin. This dispersion curve is used in an evolutionary algorithm (Luu, 2023) to iteratively solve for the best fitting 1-D function (B).

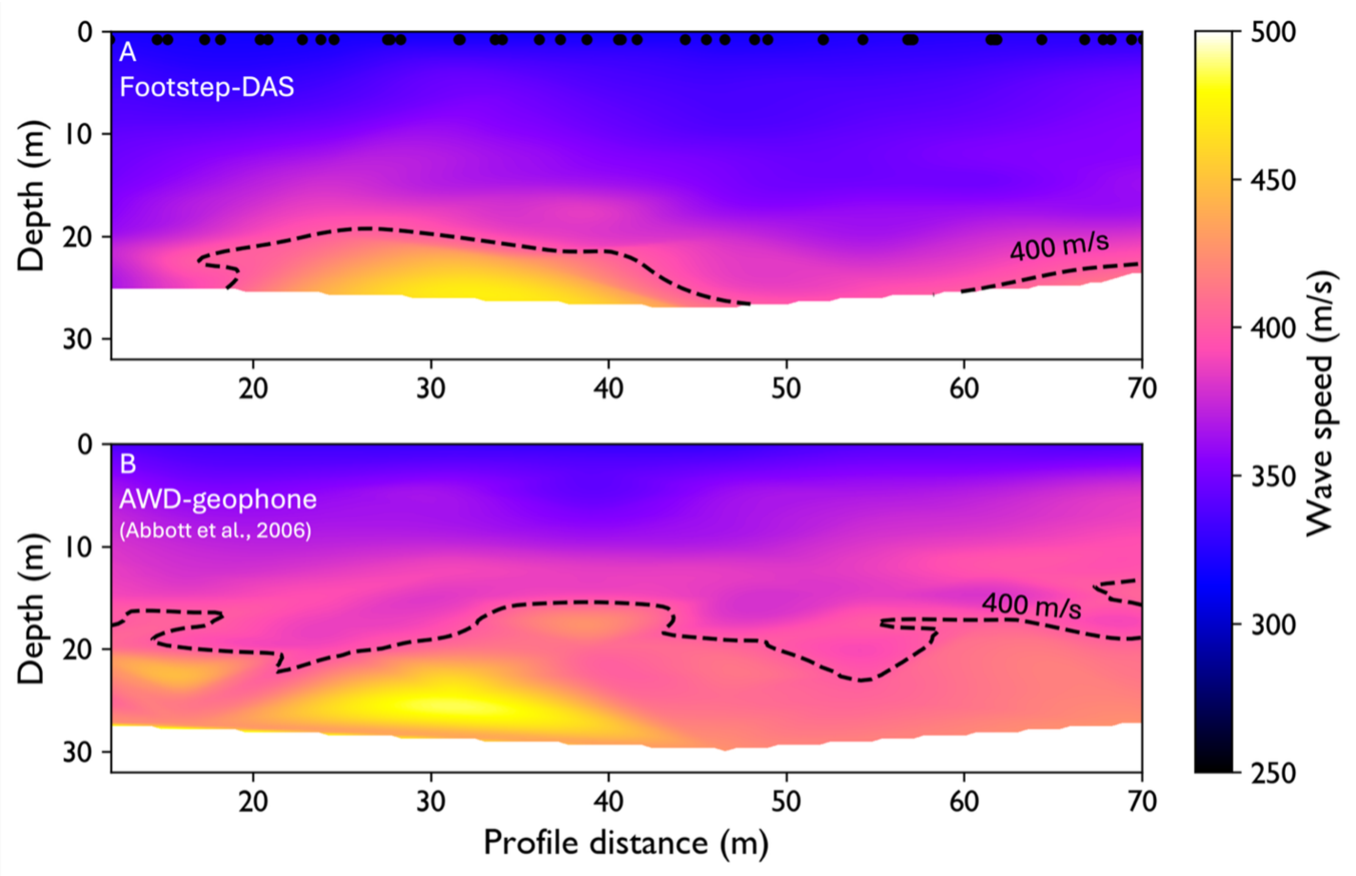

Figure 6 Shallow 2-D Vs profiles from the FACT site. Our Vs calculation (A) is comparable to Abbott et al. (2006) result (B). Black circles show locations of footsteps used in this analysis. See Figure 9B for our wave speed uncertainties.

and returning to the surface at sufficient amplitudes for observation seems unlikely. Rather, it is possible that the footstep energy is reflecting off an intermediate soil horizon above the bedrock. Migrating the deepest bright and interpretable reflector yields a depth of ~25 m, which may represent the limit of footstep reflection imaging for this site. Thus, a boundary at 15-20 m depth would be near the edge of what is resolvable using footstep sources.

6.3 Relevance to Vs30 analysis

Using our 2-D Vs profile, we can estimate Vs30 by time-averaging integrated wave speeds over the top 30 m. Since our profile does not reach 30 m depth, we extended the lowest velocities vertically down to 30 m. From our 2-D profile, we estimated a Vs30 of 335±16 m/s. The profile from Abbott et al. (2006) yielded an average Vs30 of 372±9 m/s. The closest Vs30 site surveyed by

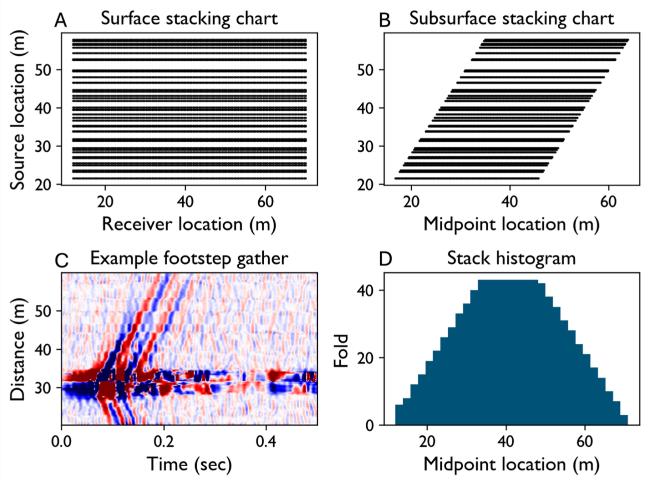

Figure 7 Geometry of footstep-DAS data. The surface (A) and subsurface (B) stacking charts graphically represent where footsteps (C) are recorded. The sum of the subsurface stacking chart produces the fold of each CDP (D).

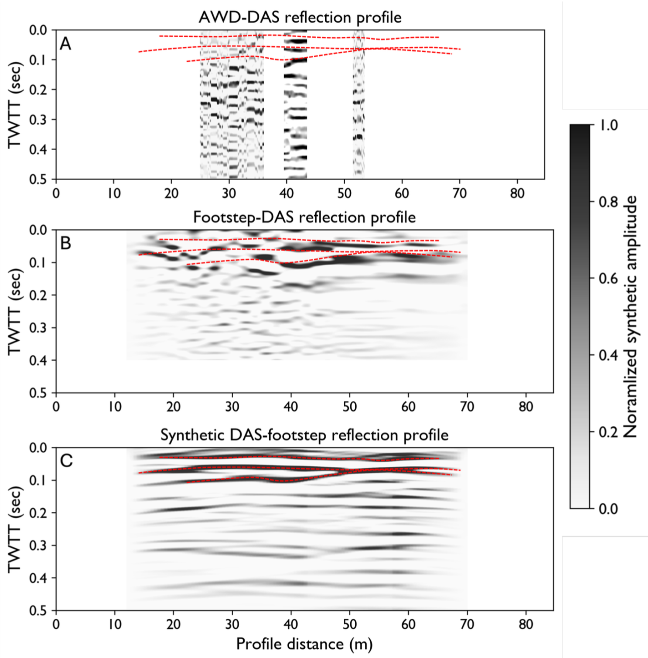

Figure 8 Reflection results with interpreted synthetic reflectors marked with red dashed lines. The AWD profile (A) is less continuous than the footstep profile (B), yet the AWD profile shows deeper propagating reflections than the footstep profile. The footstep-DAS reflection profile reveals a strong reflector at two-way travel time (TWTT) ~0.1 sec. This reflector is confirmed in the synthetic profile (C) calculated using the wave speeds from Figure 6A. All profiles are trace normalized.

the USGS reported a value of 370 m/s (McPhillips et al., 2020). As expected from the 2-D Vs comparison (Figures 6, 9), our estimated Vs30 is ~10% lower than previous results. This is consistent with wave speed ratios of ~0.9 (Figure 9A) and is likely due to differences in frequency content between footstep and AWD sources (Figure 4) or changes in shallow subsurface properties over time.

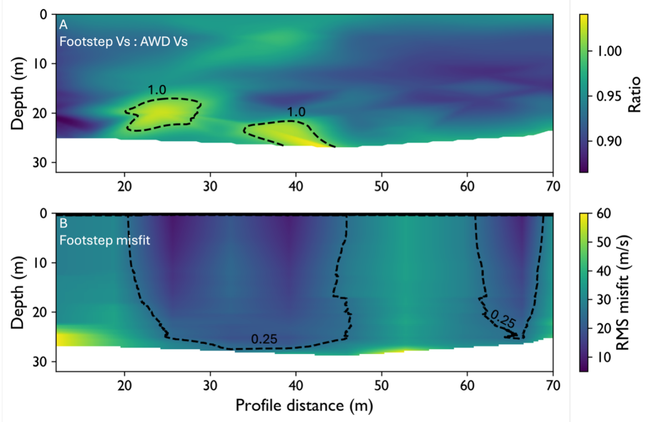

Figure 9 Validation of our wave speed calculation. The ratio between our profile and Abbott et al. (2006) shows our results are generally lower, with two regions of ratios >1.0 (A). Errors from our wave speed calculations (Figure 6A) generally fall within differences with the Abbott et al. (2006) model (B).

Additional ground truth validation of our approach could also come from the use of ambient noise interferometry recorded by DAS (e.g., Kang et al., 2025). This would independently test if footstep imaging and ambient noise interferometry produce consistent results. If consistent, this would suggest any difference between current wave speeds and those calculated by Abbott et al. (2006) are due to changes in shallow properties. Furthermore, the lower frequency content of ambient noise could provide deeper velocity information and illuminate the potential effect of footstep frequency content on wave speeds.

However, as the goal of our study was to demonstrate that DAS and footstep sources can serve as a viable alternative to traditional seismic methods, we could not perform ambient noise interferometry due to a limited data collection. Future research comparing footstep and ambient noise imaging would illuminate two useful points: (1) it would support the reliability of footstep imaging; and (2) it may further demonstrate the usefulness of footstep based methods for near-surface imaging due to data constraints (e.g., short recording periods) or environmental constraints (e.g., the quality of ambient noise in an urban environment).

Despite these uncertainties, we are still able to recover 2-D Vs, reflectivity structure, and estimate Vs30 using footstep energy recorded by DAS. This experimental setup is relevant to researchers seeking to resolve the near surface seismic structure where traditional sources and receivers may not be easily deployed. Such footstep-DAS imaging is of interest to researchers seeking to characterize urban areas, where both DAS and footstep sources are readily available. While in our experiment the footstep locations and timings were known, it is possible to locate unknown footstep locations using back-projection to accuracies comparable to GPS (Luckie et al., 2025). By estimating locations of these 'naturally' occurring footsteps, one would be able to use them as sources for traditional geophysical imaging products as we have shown here. Applying such innovative imaging to urban areas can help better constrain seismic wave speeds at a much lower cost than using traditional seismic instrumentation.

7 Conclusions

Our results demonstrate the use of footsteps recorded by DAS to characterize the shallow seismic subsurface structure. This novel method could be applied in urban environments for enhanced seismic wave speed analysis and in regions otherwise difficult to instrument with seismic sensors. The inversion of dispersion curves from footstep data yields a 2-D Vs profile congruent with existing profiles. This agreement between profiles supports the reliability of footstep sources in Vs calculations. Vs30 profile estimations are in line with expected values from previous studies. The footstep energy was also used to calculate coherent reflection images of the subsurface, demonstrating the capability of DAS to capture interpretable seismic reflections in challenging urban settings. These results underscore the potential of utilizing DAS and footstep sources in densely populated areas where traditional seismic instrumentation or active sources may be impractical. Such methods can be applied in future studies to improve the resolution of very-near surface seismic wave speed models.

Acknowledgements

We thank Haipeng Li and one anonymous reviewer for their time and effort in reviewing this manuscript.

This Source Physics Experiment (SPE) research was funded by the National Nuclear Security Administration, Defense Nuclear Nonproliferation Research and Development (NNSA DNN R&D). The authors acknowledge important interdisciplinary collaboration with scientists and engineers from LANL, LLNL, NNSS, SNL and UNR-NSL. Sandia National Laboratories is a multimission laboratory managed and operated by National Technology and Engineering Solutions of Sandia, LLC, a wholly owned subsidiary of Honeywell International, Inc., for the U.S. Department of Energy's National Nuclear Security Administration under contract DE-NA-0003525.

8 Data and code availability

The codes used for dispersion curve calculations (Park et al., 1999), wave speed inversion (Luu, 2023), and synthetic reflection calculation can be found at Sandia National Laboratories GitHub (https://github.com/sandialabs).

9 Competing interests

The authors declare that they have no competing interests.

References

Abbott, R., Bartel, L., Pullammanappallil, S., and Engler, B. *Surface-wave and refraction tomography at the FACT Site, Sandia National Laboratories, Albuquerque, New Mexico.* Aug. 2006. doi: 10.2172/891366.

Bäck, T. and Schwefel, H.-P. An Overview of Evolutionary Algorithms for Parameter Optimization. *Evolutionary Computation*, 1(1):1–23, Mar. 1993. doi: 10.1162/evco.1993.1.1.1.

Fukushima, S., Shinohara, M., Nishida, K., Takeo, A., Yamada, T., and Yomogida, K. Detailed S-Wave Velocity Structure of Sediment and Crust off Sanriku, Japan by a New Analysis Method for Distributed Acoustic Sensing Data Using a Seafloor Cable with Seismic Interferometry. Feb. 2022. doi: 10.21203/rs.3.rs-1371937/v1.

Hong, H., Yin, F., Lei, Y., Li, Y., and Wang, B. 3D near-surface P-wave velocity structure imaging with Distributed Acoustic Sensing and electric hammer source. *Earthquake Research Advances*, 4(3), 2024. doi: 10.1016/j.eqrea.2023.100274.

Jakkampudi, S., Shen, J., Li, W., Dev, A., Zhu, T., and Martin, E. R. Footstep detection in urban seismic data with a convolutional neural network. *The Leading Edge*, 39(9), 2020. doi: 10.1190/tle39090654.1.

Kang, J., Walter, F., Halter, T., Paitz, P., and Fichtner, A. Soil slope monitoring with Distributed Acoustic Sensing under wetting and drying cycles. 2025. doi: 10.5194/egusphere-2025-1725.

Li, H., Liu, J., Mao, S., Yuan, S., Clapp, R. G., and Biondi, B. L. Fiber-Optic Seismic Full Waveform Monitoring of Groundwater Dynamics. *Geophysical Research Letters*, 52(20), Oct. 2025. doi: 10.1029/2025gl117610.

Lindsey, N. J. and Martin, E. R. Fiber-Optic Seismology. *Annual Review of Earth and Planetary Sciences*, 49(1):309–336, May 2021. doi: 10.1146/annurev-earth-072420-065213.

Liu, H., Li, J., and Wang, Y. Wave Equation Dispersion Inversion of Distributed Acoustic Sensing Data. *Journal of Geophysical Research: Solid Earth*, 127(11), Nov. 2022. doi: 10.1029/2022jb024671.

Luckie, T. W., Porritt, R. W., and Baker, M. G. Applying Machine Learning and Bayesian Inference to Identify and Locate Moving Anthropogenic Sources Using Distributed Acoustic Sensing Data. *Seismological Research Letters*, 96(6), 2025. doi: 10.1785/0220250074.

Luu, K. evodcinv: Inversion of dispersion curves using Evolutionary Algorithms, 2023. doi: 10.5281/ZENODO.8141605.

McPhillips, D. F., Herrick, J. A., Ahdi, S., Yong, A. K., and Haefner, S. Updated Compilation of VS30 Data for the United States, 2020. doi: 10.5066/P9H5QEAC.

Park, C. B., Miller, R. D., and Xia, J. Imaging dispersion curves of surface waves on multi-channel record. In *SEG Technical Program Expanded Abstracts 1998*, page 1377–1380. Society of Exploration Geophysicists, Jan. 1998. doi: 10.1190/1.1820161.

Park, C. B., Miller, R. D., and Xia, J. Multichannel analysis of surface waves. *Geophysics*, 64(3), 1999. doi: 10.1190/1.1444590.

Wu, X., Willis, M. E., Palacios, W., Ellmauthaler, A., Barrios, O., Shaw, S., and Quinn, D. Compressional- and shear-wave studies of distributed acoustic sensing acquired vertical seismic profile data. *The Leading Edge*, 36(12):987–993, Dec. 2017. doi: 10.1190/tle36120987.1.

Yuan, Y., Luo, B., and Guo, Z. Deep Learning–Based Footfall Detection and Anthropogenic Activity Characterization Using Fiber-Optic Distributed Acoustic Sensing. *Seismological Research Letters*, 97(1), 2025. doi: 10.1785/0220250120.

Zhou, W., Butcher, A., Brisbourne, A. M., Kufner, S.-K., Kendall, J.-M., and Stork, A. Seismic noise interferometry and Distributed Acoustic Sensing (DAS): measuring the firn layer S-velocity structure on Rutford Ice Stream, Antarctica. 2022. doi:

10.1002/essoar.10510377.2.

Zhou, Y., Yeoh, J. K., Li, Y. E., and Solihin, W. Large scale indoor occupant tracking using distributed acoustic sensing and machine learning. *Building and Environment*, 247:111005, Jan. 2024. doi: 10.1016/j.buildenv.2023.111005.